We are IntechOpen, the world's leading publisher of Open Access books Built by scientists, for scientists

6,900
Open access books available

185,000
International authors and editors

200M
Downloads

Our authors are among the

154
Countries delivered to

TOP 1%
most cited scientists

12.2%
Contributors from top 500 universities



WEB OF SCIENCE™

Selection of our books indexed in the Book Citation Index in Web of Science™ Core Collection (BKCI)

Interested in publishing with us?
Contact book.department@intechopen.com

Numbers displayed above are based on latest data collected.
For more information visit www.intechopen.com



Chapter 1

Atomic Structure of Graphene and h-BN Layers and Their Interactions with Metals

Recep Zan, Quentin M. Ramasse, Rashid Jalil and Ursel Bangert

Additional information is available at the end of the chapter

http://dx.doi.org/10.5772/56640

1. Introduction

Since the isolation of graphene and other two-dimensional (2D) materials, such as hexagonal boron nitride (h-BN), these just one atom layer thick materials have spurred a flurry of investigations into their structural properties, morphology and chemistry [1, 2]. Graphene is a 2D crystalline form of carbon and a basic building block for carbon allotropes such as fullerenes, carbon nanotubes and graphite [3]. In graphene, carbon atoms are packed in a planar honeycomb network. The unit cell of single-layer graphene consists of two carbon atoms, separated by 1.42 Å, with a lattice constant of 2.46 Å. Each atom has s, p_x and p_y orbitals and is bonded to three neighbor atoms in the lattice, forming an sp^2 atomic network. The p_z orbitals overlap between neighboring atoms resulting in so-called filled π and empty π^* states, which respectively form the valence and the conduction bands in graphene. However, so-called Bernal (AB-) stacked double layer graphene has four electrons in the unit cell: in this configuration, the individual layers are stacked but shifted with respect to one-another, so that the carbon atoms in one layer sit on top of the empty hexagon centers in the underlying layer. Due to the absence of any measurable bandgap in both single and double layer graphene these materials are often called zero-gap semiconductors. The lack of a bandgap is a serious limitation to the use of graphene in electronics as switching off any graphene-based device would be extremely difficult. Additionally, researchers have shown that the substrate on which graphene layers are placed has dramatic effects on its transport properties. SiO_2/Si substrates were used for initial graphene devices [1]. However, due to their surface roughness and to the presence of charged impurities graphene devices built directly on SiO_2 substrates could not demonstrate any marked improvement over more traditional designs: they were seemingly never able to utilize the intrinsic properties of graphene [4]. Other substrates (2D materials)

INTECH
open science | open minds

© 2013 Zan et al.; licensee InTech. This is an open access article distributed under the terms of the Creative Commons Attribution License (http://creativecommons.org/licenses/by/3.0), which permits unrestricted use, distribution, and reproduction in any medium, provided the original work is properly cited.

such as hexagonal boron nitride (h-BN) [5] and, recently, dichalcogenides [6] have therefore been tried as support.

One of the members of 2D materials is h-BN, which consists of boron and nitrogen atoms arranged in a hexagonal structure such that each boron atom is bonded to three neighboring nitrogen atoms and *vice versa.* The resulting structure resembles graphene, with a similar lattice constant of 2.52Å. When stacked, h-BN adopts a so-called AA' configuration whereby each boron atom sits atop a nitrogen atom, and *vice versa* [7]. By contrast, graphene is most frequently observed in an AB stacking arrangement. Despite the presence of structural similarity between the graphene and h-BN structure, the electronic characteristics are totally different; graphene is a conductor (semi-metal) whereas h-BN is an insulator or a wide gap semiconductor, with a gap of 5.9 eV, which makes it the thinnest possible insulator. In addition, h-BN is mostly inert, its surfaces are missing dangling bonds, and it has large optical phonon modes, making it an ideal substrate (dielectric support) for high-quality graphene electronic devices [5]. h-BN has strong covalent bonds in the plane between the atoms and weak Van der Waals bonds between different planes, which is similar to graphene, but, the bond is slightly ionic in comparison to graphene.

Due to its unique properties, graphene can be employed in a variety of applications. It is thought it may eventually replace many of the materials currently used in today's technology and result in higher performance, energy efficiency, flexibility and durability [8]. Graphene is being used in electronics [9], energy storage [10, 11], photonics [12], composite materials [13], sensor technology [14] and as a sample support for TEM applications [15]. One of the most promising electronic applications of graphene is the manufacture of transistors [1]. However, transistors, as any other graphene-based electronic device, must involve the incorporation of metal contacts, which link the graphene to the other device components. The choice of the metal used as a contact has been shown to dramatically affect the performance of the resulting devices [16], with little understanding hitherto of why this is the case. While the macroscopic properties of graphene devices are readily measured and characterized, understanding the metal-graphene interactions necessitates an investigation and direct 'visualization' at the atomic level, which is a remarkably challenging task. Indeed, there are only few reported observations at the atomic scale of the metal-graphene system, especially for suspended (or 'free-standing') graphene. A large effort has in fact been recently devoted to suspended devices [17, 18]. Using suspended graphene (rather than supported on a different material) eliminates substrate effects, which are known as a limiting factor for the mobility in graphene based devices [19]. A fully suspended geometry also allows exploiting directly the intrinsic, exceptional properties of the material. It is thus essential to carry out detailed systematic studies of the nucleation following deposition, and of the resulting coverage of metals on suspended graphene, in order to determine what the optimal contact might be and ultimately to improve device performance.

Transmission Electron Microscopy (TEM) or Scanning Transmission Electron Microscopy (STEM) are an ideal, perhaps the only, tool for such studies. Indeed, the technique's ability to image and identify directly each and every atom in 2D materials has already played a significant role in improving our understanding of graphene properties [20, 21]. Rapid

progress in microscope components in recent years, in particular the successful implementation of aberration correctors for electron optical lenses, has heralded a new era in materials- and nano- science research. These instrumental advances have substantially improved the overall performance of electron microscopes: much higher resolutions are now attainable in both structural and spectroscopic data, with very clear benefits to the understanding of the investigated material's structure. More crucially, they enable the use of much lower acceleration voltages, e.g., <80 keV, below the carbon knock-on threshold (voltages, typically ranging from 100 to 300kV, have conventionally been used to accelerate the electron beam towards the specimen inside the microscope column) whilst maintaining atomic resolution. Structural changes and damage to the specimen due to its interactions with the high energy electron beam can thus be reduced without losing any of the structural details in the micrographs. Most of the results presented in this chapter were obtained on a Nion UltraSTEM microscope. The microscope was operated at 60 kV acceleration voltage to prevent knock-on damage to the graphene [22]. High angle annular dark field (HAADF) imaging was employed to produce micrographs. This chemically-sensitive 'Z-contrast' mode is ideally suited to directly identify the nature of individual atoms and it is usually complemented by further chemical fingerprinting through Electron Energy Loss Spectroscopy (EELS).

In the following in turn, we will summarize fabrication of graphene and h-BN flakes, their preparation for microscopy measurements, pristine graphene and h-BN S/TEM characterization, metal doped graphene and h-BN characterization and finish by conclusions.

2. Graphene and h-BN fabrication

Two different techniques were used to produce the graphene membranes for the experiments: mechanical cleavage of highly ordered pyrolytic graphite (HOPG) and chemical vapor deposition growth on copper substrates. For h-BN fabrication only the former method was used. Obtaining graphene and h-BN by exfoliation (mechanical cleavage) is simply done by pressing a piece of HOPG or bulk h-BN crystal against some adhesive tape and peeling the tape off [1, 23, 24]. Due to the layered structure of graphite and h-BN and the weak interlayer bonding (Van der Waals), the layers are easily separated, so that after repeating the peeling process a few times extremely thin layers are left on the tape. The thin graphite and h-BN flakes obtained in this fashion are then placed onto an oxidized silicon substrate. The obtained layers are initially observed under the optical microscope to identify single layer regions, whose specific color and contrast against the oxidized silicon wafer background provide a quick and convenient screening criterion. Identification of graphene flakes on the wafer is straightforward. An optical micrograph of exfoliated graphene layers on an oxidized silicon substrate is presented in figure 1. The flakes on the wafer vary in thickness from single layer to much thicker regions: a single layer area, 100x100μm in size, is magnified. This size of the single layer graphene flake is adequate not only for electron microscopy but also for many other characterization techniques. However, due to their weak contrast on the wafer and their small size compared to graphene, identification of h-BN flakes under the optical microscope is a quite challenging task.

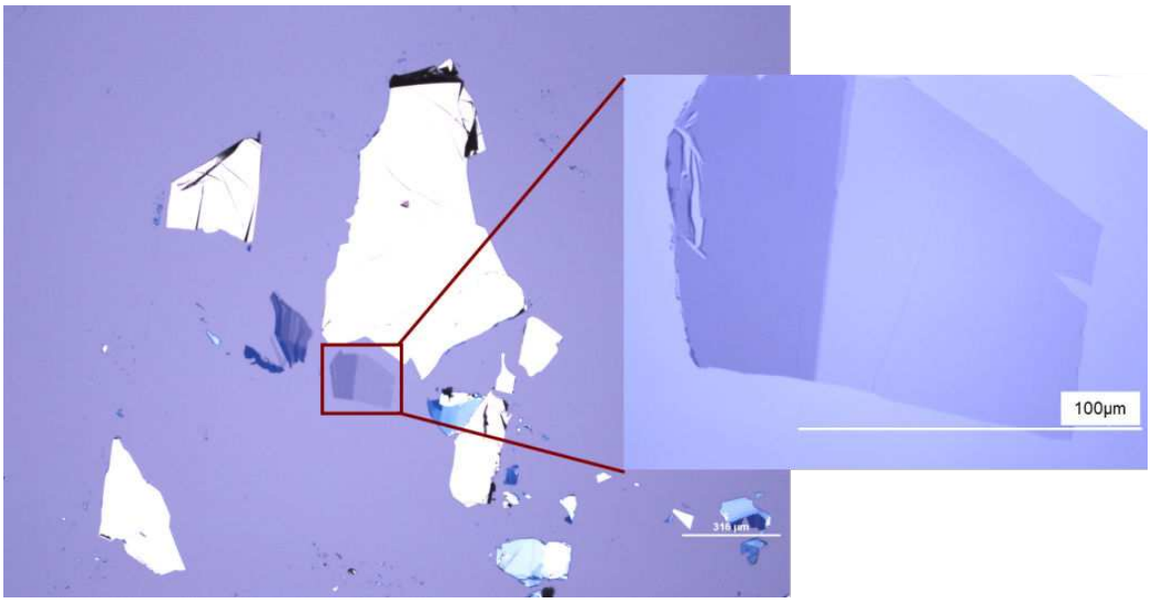


Figure 1. Optical image of the exfoliated graphene layers on 290 nm thick oxidized silicon wafers and enlarged view of single layer region, shown as inset.

Graphene growth by the chemical vapour deposition (CVD) technique is based on the decomposition of hydrocarbon gases at elevated temperature and the diffusion of carbon atoms ona metal surface, followed by rapid cooling to 'freeze in' any graphene layers formed on the surface of the substrates. The most widely used combination of gas and substrate at present consists of methane gas and a copper substrate; the low solubility of carbon in copper provides a means of restricting the graphene growth to a single layer [25, 26]. In our case, graphene was obtained on Cu substrates and methane gas was used as precursor in a quartz tube at pressure 600mTorr.

2.1. Fabrication of suspended sample for microscopy

A so-called *wet transfer* technique was used to prepare suspended samples for the microscopy experiments from both exfoliated and CVD-grown flakes, with only small variation in the methodology depending on how the flakes were initially grown [27, 28].

In the case of exfoliated samples for both graphene and h-BN, following the initial identification of regions of interest on the oxidised silicon wafer under an optical microscope, a layer of ~300 nm of poly-methyl-methacrylate (PMMA) was 'spun' onto the graphene flakes using a spinner, followed by a 130°C bake of the samples for 5mins. This additional layer is designed to protect the underlying graphene layers, providing mechanical support and facilitating the handling of the flakes during the transfer procedure. The substrate, or more precisely the oxidised silicon layer (topmost layer of the wafer), is then etched away using a 3% potassium hydroxide (KOH) solution, detaching the PMMA and the flakes from the silicon wafer. Once almost detached, the wafers are dipped into de-ionized (DI) water, to fully detach the PMMA and the flakes and to rid them of chemical residues from the etching process as well as of any possible contamination from the silicon wafer. Rinsing in DI water is repeated to ensure the

http://dx.doi.org/10.5772/56640

best sample cleanliness. Once the flakes are transferred onto a TEM grid by simply 'fishing them out' of the DI water bath, the sample is dried at 50°C for 10 mins, followed by a further 120°C bake for 10 mins in clean room conditions to improve the adhesion of the flakes to the grid, get rid of any remaining water content, and importantly, to flatten out (anneal) any possible wrinkles, which may have been created during the transfer. The PMMA protective layer is then dissolved by dipping the sample into acetone for 15 mins. Finally, the sample is dried in a Critical Point Dryer (CPD) in order to protect the delicate, now suspended, graphene layers against any rupture, damage or deformation due to surface tension. The transfer process to TEM grid is schematically summarised in figure 2.

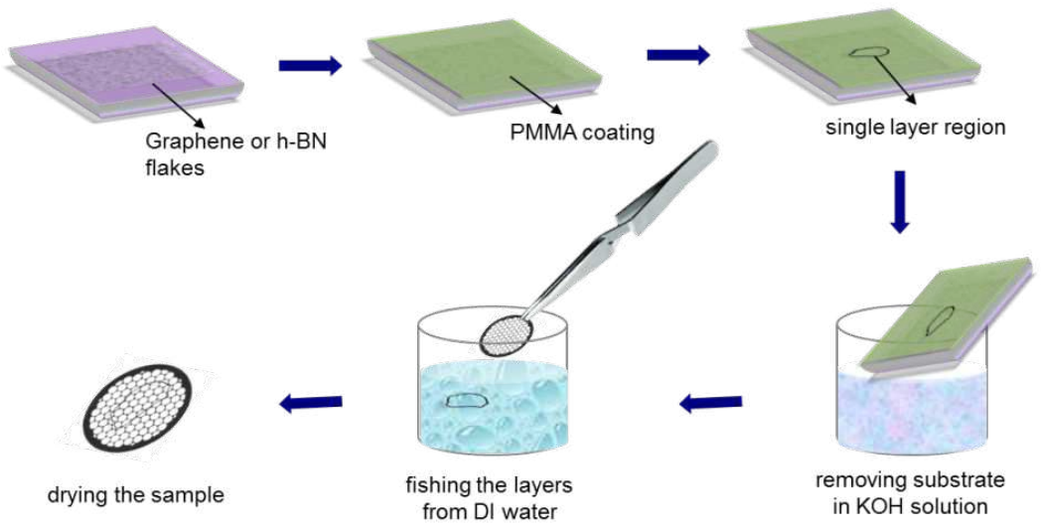


Figure 2. Schematic representation of the transfer of exfoliated graphene layers from an oxidized silicon wafer to a TEM grid by wet-etching using a KOH solution.

Optical images of exfoliated graphene flakes on the substrate (figure 3a) and after transfer onto the grid are shown in figures 3b and c, along with a low magnification TEM image in figure 3d.

In the case of graphene obtained by CVD on Cu substrate, the graphene growth takes place on both sides of the Cu surface. An additional step is therefore necessary to remove the flakes present on one of the two sides to avoid interference of layers during the transfer. The side being prepared for transfer is covered with PMMA, in order to protect the underlying graphene and to ease the transfer process as was the case for exfoliated samples, while the other side is exposed to a 20 mTorr oxygen plasma for a few minutes to remove the graphene layer. Then an aqueous ammonium persulphate ($(NH_4)_2 S_2O_8$) solution (0.1 molar) was used to etch the Cu substrate to produce the material investigated here. After the etching procedure, the PMMA/graphene layers are repeatedly rinsed in DI water, to remove further possible contaminants. The flakes are again directly transferred onto TEM grids by 'fishing them out' of the DI water bath. As for the exfoliated graphene transfer procedure previously described, the grids are then baked, the PMMA layers are dissolved in acetone and finally dried in a CPD.

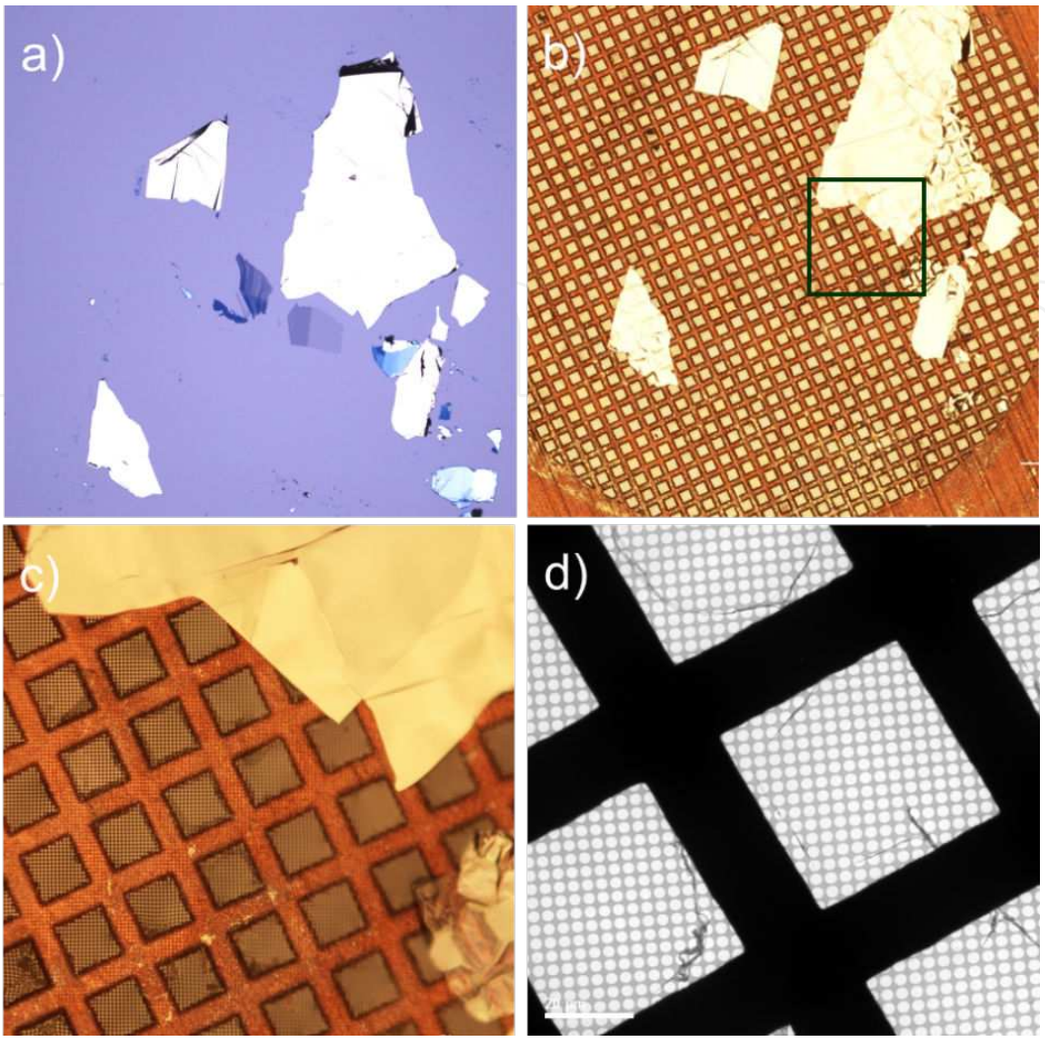


Figure 3. Graphene flakes a) as prepared on an oxidized silicon wafer, b) after transfer onto a TEM grid; c) magnified optical image of the green square indicated in (b) illustrating how suspended single layer regions are not easily visible; d) low magnification TEM image of a single layer area. Broken flakes and rolled up regions produce some visible contrast and hint at the presence of the single layer graphene sheet.

Thermal and electron-beam evaporators were used to deposit metal impurities onto the suspended graphene membranes. A fixed amount of material was deposited in fixed conditions for a large variety of metallic species, allowing a thorough comparison between metals, of the distibution, size and shape of the clusters. A total amount of 2Å of Au, Ti, Ni, Al and Pd was evaporated onto different suspended graphene and h-BN layers on TEM grids at a rate of 0.1 nm/s, in vacuum better than 10^{-6} mbar (up to ~10^{-8} mbar).

3. Transmission electron microscopy

Electron microscopy is based on the interactions of matter with a high energy beam of electrons (from a few keV to several 100 keV). These interactions provide insights about the structure,

topology, morphology and composition of a material. The interactions of an electron beam with matter can be divided into two categories: *elastic* and *inelastic* interactions, which are used in the TEM and STEM to obtain structural and compositional information about the specimen.

One of the main imaging modes of a TEM is known as bright field (BF) in which only the direct, unscattered and small-angle scattered electrons are allowed to contribute to the image formation. Phase contrast is the main contrast mechanism in BF imaging and constitutes the basis for so called high-resolution TEM (HRTEM). Phase contrast occurs due to the difference in the phase of the electron waves inferred by interaction with the atomic potential of the atoms in the thin specimen.

3.1. Scanning transmission electron microscope

In contrast to employing a broad and stationary beam in conventional TEM, in the STEM a small, focussed probe is scanned over the specimen. Transmitted or scattered electrons are collected to build up images serially from a very large number of image points over a reasonably long time (for high signal/noise ratio), whereas in a TEM image recording is parallel (simultaneous for all image points) and thus usually much shorter.

A STEM is more powerful to obtain Annular Dark Field (ADF) images than a conventional TEM. One of the most important characteristics of ADF imaging is using incoherent, elastically scattered electrons in contrast to BF imaging which relies mostly on phase contrast and therefore interference phenomena. STEM ADF signals are predominantly produced by electrons that have been scattered by the atomic nucleus (Rutherford scattering). This makes the ADF intensity of individual atoms depend on the charge of the atom's nucleus. Different Z atoms therefore give different ADF image intensities and this imaging technique is called Z-contrast imaging [29]. Only when sufficiently high angles are used in STEM ADF imaging does it become predominantly incoherent. This imaging (collecting very high angle, incoherently scattered electrons) is also often called HAADF imaging as the intensity recorded in this mode by positioning the electron beam on an atomic site is approximately proportional to the square of the average atomic number Z of this site [30, 31]. The HAADF-STEM imaging mode is particularly useful to visualize the structure and defects of materials, as its chemical sensitivity provides a direct visual guide to identify ad-atoms and impurities of a different weight from the surrounding material [22, 32].

As a result of inelastic interactions between the incident beam and the specimen, the scattered electrons can lose a part of their energy. This loss of energy can be measured by a spectrometer to yield elemental, chemical and dielectric information about the specimen. In addition to HAADF imaging, EELS was employed to identify foreign species on the graphene and h-BN surfaces in our investigations.

3.2. Instrumenation

Tecnai: Initial experimental data to identify graphene layers and some of the high resolution data of the metal-graphene system were obtained on an FEI Tecnai F30 microscope operated at 300 kV.

SuperSTEM: Most of the experimental data were acquired on an aberration corrected dedicated STEM, the Nion UltraSTEM It is equipped with a cold field emission gun with an energy spread of 0.3 eV and operated at 60 kV to prevent knock-on damage in graphene. The UltraSTEM microscope has a UHV design throughout, allowing pressures at the sample of below $5x10^{-9}$ torr for contamination-free observation. The estimated probe size (full width at half-maximum) is about 1.2 Å for the typical operating conditions for graphene investigations at 60 kV acceleration voltage and 30 mrad probe convergence semi-angle. Detectors with different geometries are used to collect electrons scattered to different angular ranges. For example, the BF detector used to obtain phase contrast images can collect electrons scattered up to 6 mrad. The so-called medium angle annular dark field (MAADF) detector collects electrons scattered from 45 to 190 mrad and the HAADF detector used to record the Z-contrast images has inner and outer radii of 70 mrad and 210 mrad, respectively. The instrument is equipped with a Gatan Enfina EEL spectrometer and its acceptance semi-angle was calibrated at 35 mrad for core-loss spectroscopy.

4. TEM characterisation of pristine graphene

TEM has been widely used in graphene research for applications as varied as: number of layers determination [33], elemental identification [22, 34], surface roughness (ripples) visualization [33, 35], detection of sheet edge types [36], observation of defects [37], and stacking faults [38, 39], impurities, such as contamination and individual ad-atoms [40] effects of radiation [41] and investigation of graphene based heterostructures [42].

Due to the substantial amount of hydrocarbon contamination, foreign ad-atoms and other residues from the chemicals used during fabrication and transfer, graphene layers were found not to be perfectly clean as also evidenced by low magnification STEM micrographs. Although the presence of contamination can be reduced with careful and cleaner fabrication and transfer procedures, 'unintentional' contamination (due to handling of the samples in air or to residual gases in the microscope column [21] albeit to lower amounts), was observed to exist on the surface at all times. An unprocessed HAADF image of a reasonably large area of a single layer graphene flake is shown figure 4a. It can be clearly seen that clean graphene regions (residue free areas) are limited in size (from few to few hundred nm^2) and surrounded by contamination, which was found to consist of H, C, O and Si in our EDX analysis. Very dark, grayish and bright regions in the image represent the graphene, hydrocarbon contamination and foreign ad-atoms, respectively. Contaminations are also clearly visible due to higher scattering in regions with heavier atoms and larger thickness. A close-up of figure 4a is presented in figure 4b which shows the atomically resolved graphene lattice.

TEM electron diffraction is a straightforward technique to distinguish single- from double- and few-layer graphene by comparing the intensities of the first and second ring of the diffraction spots [20, 33]. For single layer graphene the intensity of the outer hexagon spots is roughly the same as, or less than that of the inner one. In contrast, for double layer graphene the outer hexagon intensity is higher than the inner one. Figure 5 shows diffraction patterns

http://dx.doi.org/10.5772/56640

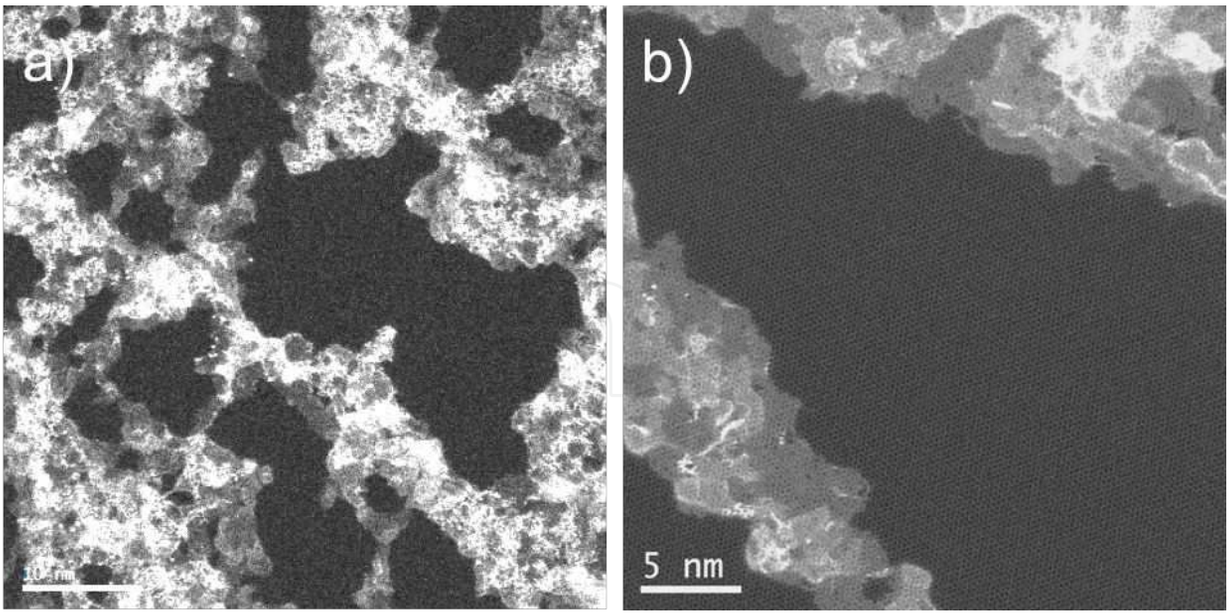


Figure 4. a) An overview unprocessed HAADF and b) High resolution HAADF image of pristine single layer graphene.

for single- and AB-stacked double- layer graphene and their intensity profiles. In addition, diffraction peak intensities vary only weakly with the tilt angle between the graphene membrane and the incident beam for single layer graphene, whereas for double layers, tilting of a few degrees leads to strong variations in the diffraction intensities [20].

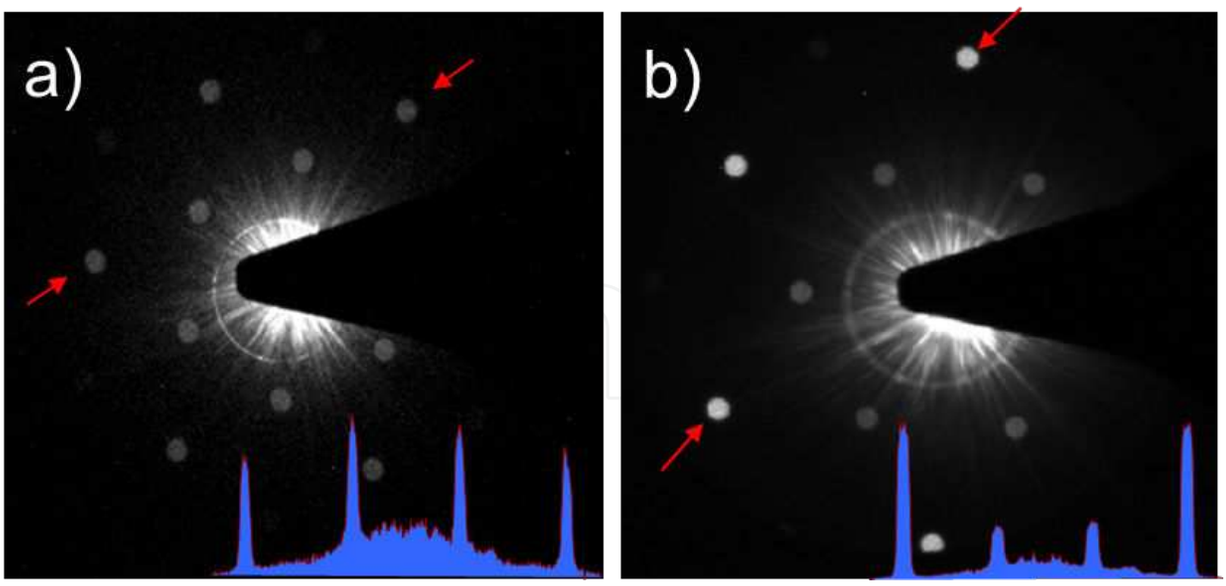


Figure 5. Diffraction patterns of a) single layer and b) double layer graphene. Intensity profile plots taken between the red arrows are shown in the inset. The diffraction patterns were acquired with a Tecnai F30.

After identifying single layer graphene, high resolution BF and HAADF micrographs were recorded. Although both BF and HAADF images can be used to visualize the graphene

structure, HAADF images are more powerful to identify individual atoms in the lattice due to its approximate Z^2 sensitivity. Thus, atomic resolution STEM was used to visualize the hexagonal atomic structure of graphene as well as individual carbon atoms in the graphene lattice. Atomic resolution STEM- BF and HAADF images of single layer graphene are shown in figures 6a and d, respectively. Although the images are unprocessed and acquired at 60 kV, the hexagonal structure and individual carbon atoms, especially in the HAADF image, are visible. Carbon atoms appear bright and holes dark in the HAADF image and *vice versa* in the BF image. Simulated BF and HAADF images with the respective STEM parameters are also shown in figures 6b and c, respectively. The simulations were performed with the Kirkland TEMSIM program using multislice method to calculate the electron wave function exiting the specimen [43].

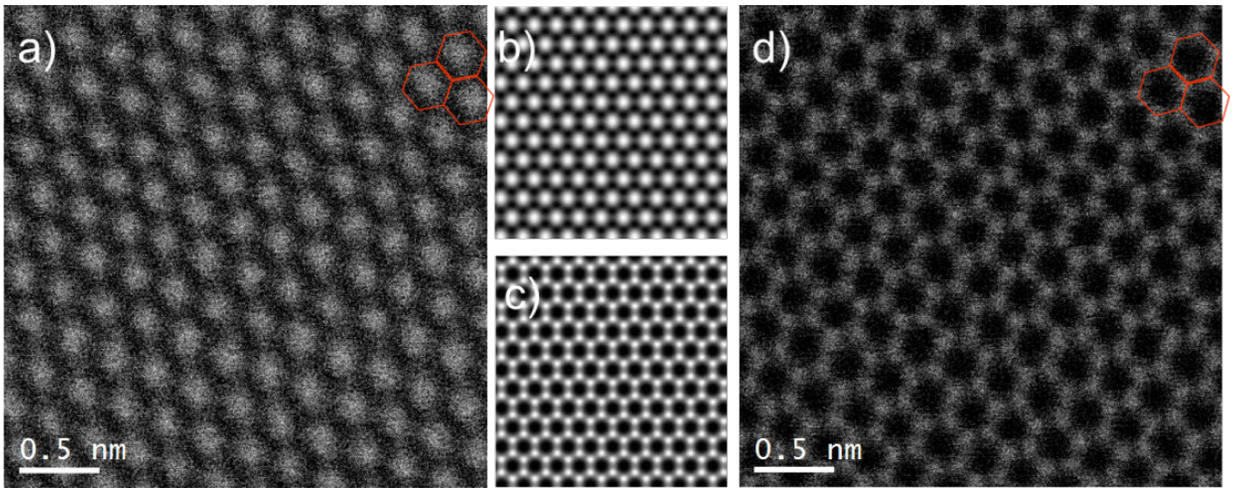


Figure 6. Unprocessed atomic resolution a) experimental raw BF, b) simulated BF, c) simulated HAADF and d) raw experimental HAADF images of pristine single layer graphene at 60kV.

HAADF images are found to be very useful for observing foreign ad-atoms on/in pristine graphene and most of them can be identified via intensity/contrast analysis by utilizing the sensitivity of HAADF images to the atomic number [22, 32]. However, HAADF imaging in combination with EELS dramatically increases the accuracy of chemical analysis. For example, Si, one of the most abundant and stable contaminants in graphene, was observed and identified by simultaneous HAADF imaging and EELS analysis shown in figure 7. The point spectrum was taken on the red circled bright atom, which was identified to be Si by its $L_{2,3}$ absorption edge.

Diffraction patterns are also utilized to identify and observe disordered or misoriented graphene membranes known as turbostratic graphene. This misalignment in between layers might be formed during exfoliation of graphene with different orientations on top of each other or during the growth process, in particular for graphene grown on nickel substrates. However, it is not perfectly clear whether they originate from the fabrication process or intrinsic stacking faults. The turbostratic graphene layers were easily identified by multiple diffraction spots in the diffraction pattern. Rather than having only 6 spots in each ring as in the case of single and

http://dx.doi.org/10.5772/56640

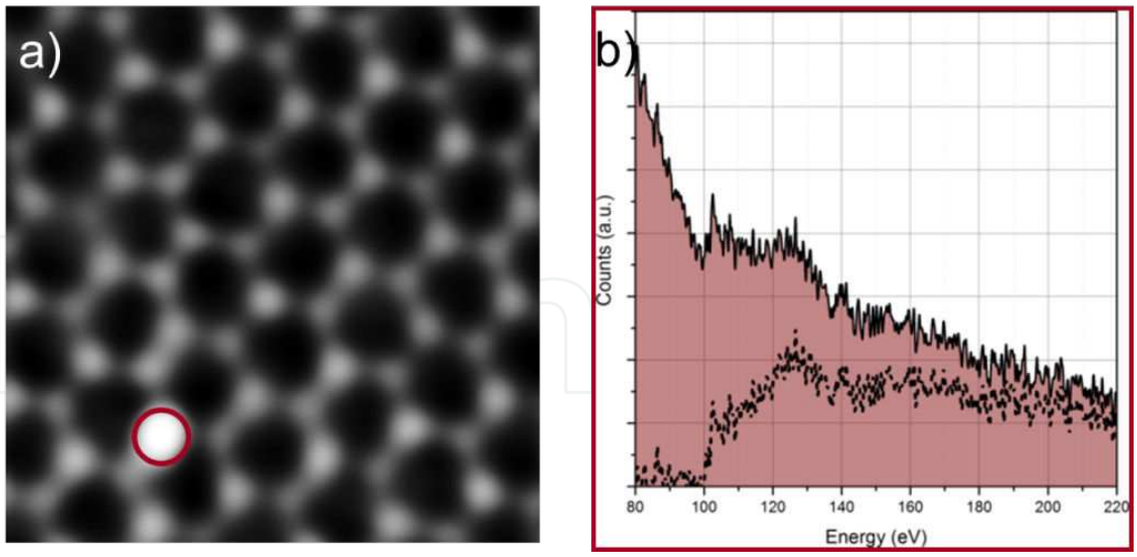


Figure 7. a) Noise filtered HAADF image of single layer graphene with bright atom at bottom left side, b) EEL spectra taken on the red circled bright atom in a) and background subtracted spectra shown as dotted line revealing that the bright atom is Si.

Bernal-stacked few layer graphene, several sets of 6 spots appear for misoriented layers (6, 12, 18 etc.) where each 6-spot pattern represents one layer [38]. The rotation angle between the layers can be determined by measuring the angle between neighboring diffraction spots in the same ring of the diffraction pattern and the angles between the layers have been found to vary from 1° to 59°. The angle between neighboring spots in the same ring of the diffraction pattern (hexagonal) of graphite (graphene layers) is 60°. Thus when the rotation angle between layers is 60° the spots from different layers overlay and rotation cannot be distinguished. When graphene layers are rotated with respect to each other it gives rise to Moiré patterns in which a larger periodicity is superimposed onto the single- or AB-stacked multi- layer graphene. It has been demonstrated both, theoretically and experimentally, that the graphene layers become electrically decoupled when the layers are misoriented [44]. The parabolic band behavior of AB-stacked double layer graphene changes to a linear dispersion when the layers are decoupled, meaning a change in the electronic structure upon layer rotation. Additionally, an external electric field does not open a band gap in the spectrum in case of turbostratic double layer graphene unlike in AB-stacked double layer graphene.

A diffraction pattern for turbostratic double layer graphene is shown in figure 8a. There are 12 spots in each ring rather than just 6 and each group of 6 spots arises from different layers. The rotation between layers is 12° as measured from neighboring spots. Although diffraction patterns can be used as a straightforward method to identify the presence of turbostratic graphene, it is important to witness the Moiré pattern at a reasonably high magnification because single, double (AB-stacked) and turbostratic graphene layers appear quite similar to each other when observed at low magnification. High magnification atomically resolved BF images of turbostratic double layer graphene are shown in figures 8b-d and rotation angles are measured as 5°, 8°, 15° for b, c, and d, respectively form their Fourier transforms shown as

insets. As can be seen in figures 8b-d, the Moiré periodicity in the turbostratic graphene is larger than the lattice periodicity of single layer or AB-stacked few layer graphene [45]. Additionally, the periodicities are getting smaller as the rotation angle between the layers increases. Furthermore, individual graphene layers of turbostratic graphene can be reconstructed as shown in figure 8e and f by masking different sets of hexagonal spots as shown in the inset. The sum of the separate (reconstructed) images in figures 8e and f is then shown as inset to make sure the reconstruction of layers led to the correct image.

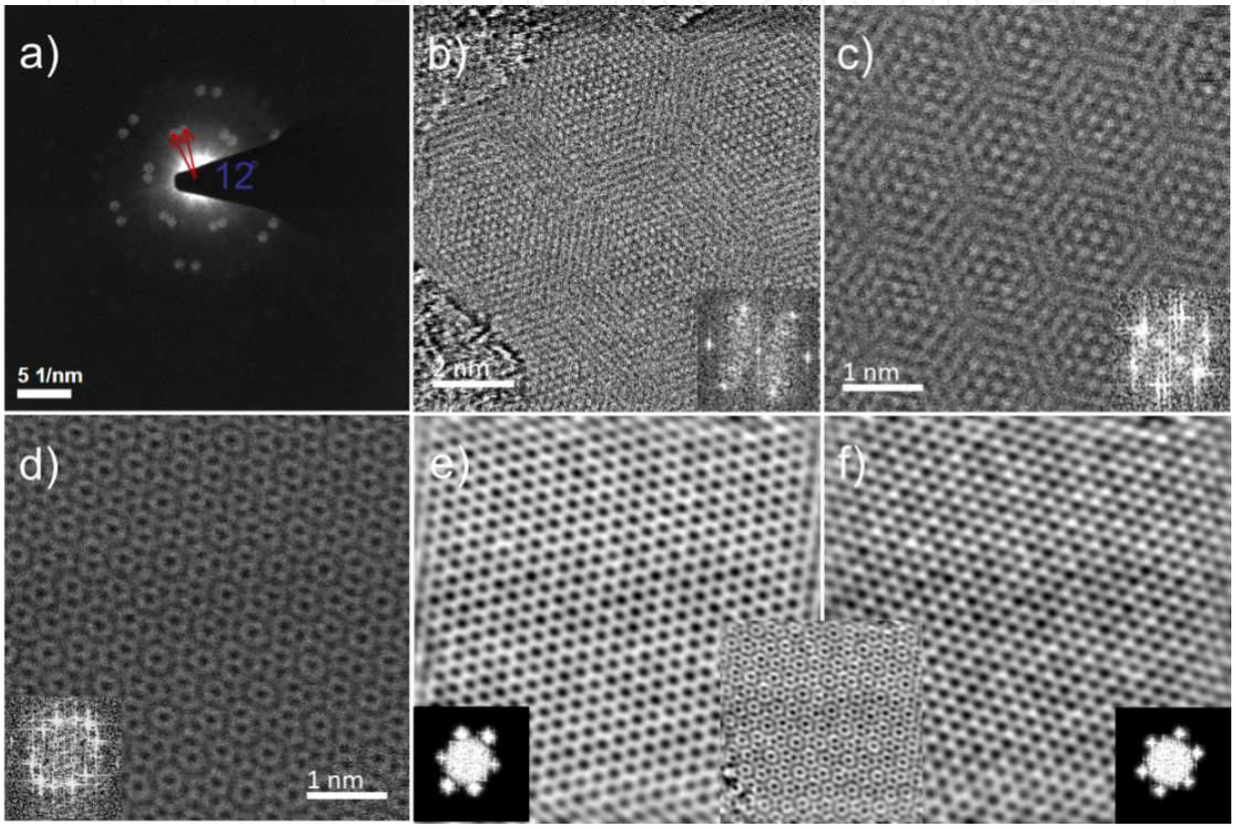


Figure 8. a) Diffraction patterns of turbostratic graphene, the angle between the spots is 12°; b). c) and d) turbostratic double layer graphene unprocessed BF images taken at 60kV with rotation angles between the layers of, respectively, 5°, 8° and 15° ; the rotation angles are measured on their respective FFTs, shown insets. e) reconstructed first layer by masking 6 spots in the FFT (inset), (f) reconstructed second layer by masking the other 6 spots (inset), and summed reconstructed layers (inset).

5. TEM characterisation of pristine h-BN

Single layer h-BN HAADF experimental (raw and filtered) images are presented in figure 9. B and N in both images are easily discernible as the atomic number of N is higher than B and thus N atoms appear more intense than B atoms; this gives triangular patterns. For a better demonstration of the difference between B and N, a part of figure 9a is filtered and magnified

http://dx.doi.org/10.5772/56640

as shown in figure 9b. The B-N sequence can also be revealed by the intensity profiles, e.g., like the one taken along the red line in the filtered image that shown in figure 9c.

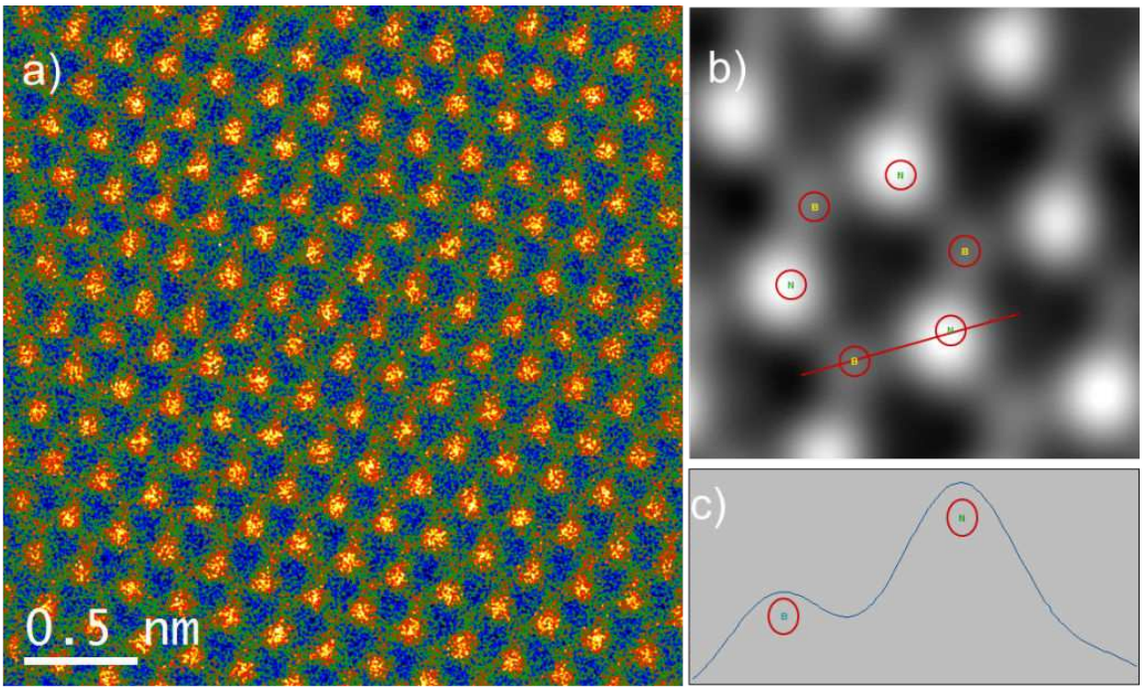


Figure 9. HAADF single layer h-BN images at 60 kV. (a) unprocessed (color inverted), (b) filtered (and magnified of a), (c) B and N can be distinguished as demonstrated by the intensity profile across the image (b).

AA' stacking is the well-known stacking configuration for h-BN, with boron on top of nitrogen and vice versa. AA' stacked double layer h-BN is shown in figure 10a. As can be seen the intensities in neighboring atomic positions are similar to each other due to the same number of atoms giving the same sum of Z^2 in the atomic columns. Although imaging was performed at and energy of 60 keV, which is lower than the calculated displacement threshold energy for the atoms in the h-BN structure, we were able to etch thick h-BN region layer-by-layer with the scanning electron beam. An example of this is shown in figure 10b, which was taken few minutes after figure 10a. The etching happened in triangular shapes as is always the case for h-BN because of the difference in the knock-on threshold energies of B and N [7, 46]. As a result of etching, a single layer region appeared revealing itself by the above mentioned triangular intensity pattern (see figure 10b).

Misorientations are also observed between h-BN layers similar to graphene, giving rise to Moiré patterns, which reveal themself by multiple spots in diffraction patterns or in Fourier transforms of the micrograph [39]. A noise filtered STEM-BF image of double layer turbostratic h-BN is shown in figure 11a. A magnified image of the red square in figure 11a is presented in figure 11b, which provides a closer look into turbostratic appearance of h-BN layers. The rotation angle between the layers was found to be 6° from measurements of the angle between neighboring spots in the Fourier transform as shown in figure 11c.

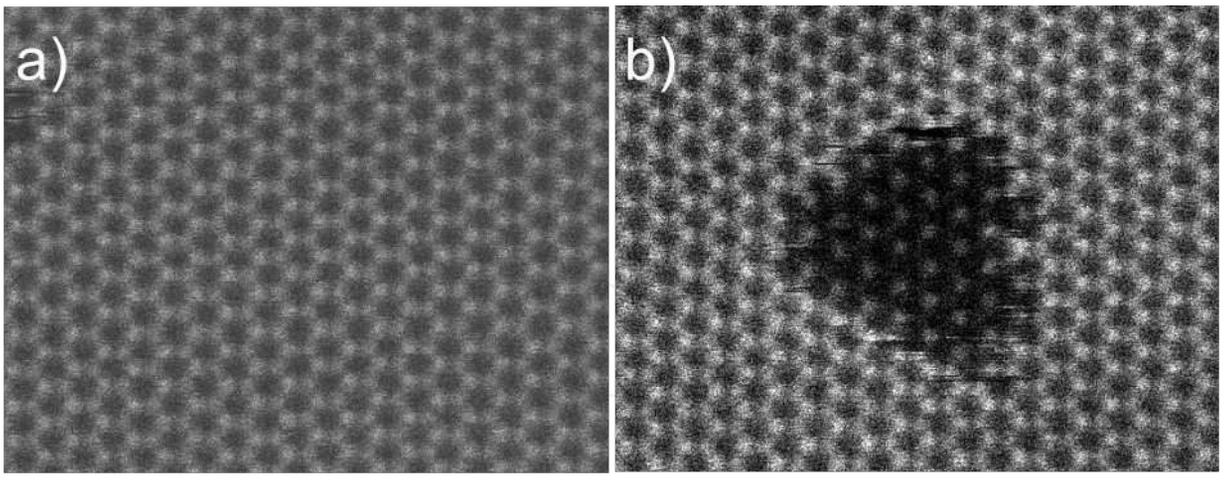


Figure 10. Unprocessed HAADF double layer h-BN images at 60 kV a) before and b) after electron beam induced etching, revealing a single layer region.

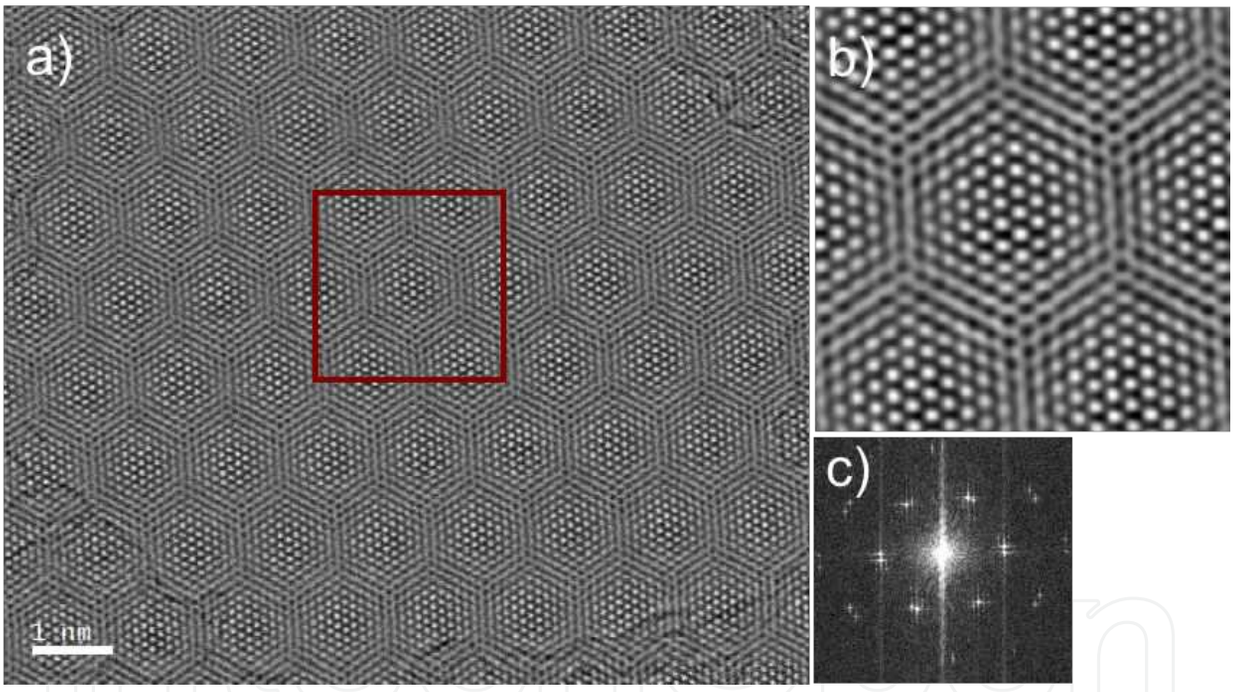


Figure 11. a) Unprocessed STEM BF image of turbostratic h-BN, b) magnified and c) FFT of (a).

6. Metal-graphene interactions

Any electronic device irrespective of whether macro or nano sized has metal contacts to connect it to external device components. Thus, metal behavior on material surfaces is an important subject of study. The interfacing of graphene with metal contacts is a recurring theme for graphene based devices. This area of graphene research is still ripening and the

consequences of particular dopants on graphene's electronic properties are still being investigated. Understanding of metal-graphene interactions on a fundamental level is of significance to the improvement of graphene based devices. Thus, distribution, bonding, doping and stability of metals on the graphene surface needs to be understood. For this purposes we studied various metals on single and few layer graphene.

Figures 12a and b shows simultaneously taken BF and HAADF images of 2Å gold evaporated on single layer graphene. Gold atoms and clusters segregate to the hydrocarbon contamination, which indicates the extreme mobility of gold on the residue free pristine (clean) graphene surfaces (upper right corner of figures 12a and b).We never observed gold atoms on single or misoriented (turbostratic) graphene layers [47]. Single gold atoms can only be observed on few-layer graphene films, where the bonding contribution from sub-surface layers appears to suppress their diffusion and enhance the sticking probability to the graphene surface. The gold atoms, which have appeared on few-layer graphene (figures 12c and d; some of them are numbered), were dissociated from the bigger gold cluster (left, figure 12d) as a result of repeated scanning in the STEM [48]. The atoms stay for a few scans in their positions. By comparing locations of gold atoms in the HAADF image (figure 12d) with identical positions in the BF image, (figure 12c), the sites can be identified as on top of carbon atoms in the graphene honeycomb structure. The position of metal impurities with respect to the hexagon structure depends on the metal's electron affinity and the electron density on the hexagon structure; these factors determine whether gold atoms sit on top of carbon atoms, on the bond bridging two carbon atoms or centered at the middle of the hexagon.

Initial investigations of gold atoms on pristine graphene revealed that none of the metals studied reacted with the clean (residue free) graphene surface. Thus to be able to amend this behavior researchers proposed to attach hydrogen to carbon atoms in the graphene lattice. Hydrogen ad-atoms can trap small molecules to specific sites on the graphene surface and these molecules remain stable at room temperature [49]. This suggestion stimulated attempts of experimental proof of gold deposition on functionalized graphene with hydrogen [48]. Hydrogenation breaks graphene sp^2 bonds and leads to sp^3 bond formation, which leads to opening of a band gap. We have carried out gold deposition on hydrogenated graphene surfaces to find out whether the latter increase the sticking probability for gold atoms. To conduct a fair comparison, gold evaporation was performed for the same amount (2Å) and simultaneously on hydrogenated and pristine graphene surfaces. TEM-BF images of gold deposited pristine and hydrogenated graphene taken at the same magnification are presented in figures 13a and b, respectively. As can be seen in the figure the hydrogenated sample has a higher gold coverage, and gold cluster distributions and cluster sizes are of higher uniformity than in the pristine graphene sample. In the latter case less than half of the area is covered with gold and cluster sizes vary. However, similar to pristine graphene, gold is only retained in the contamination on the hydrogenated sample [48].

In the process of investigating the interaction between metal species and graphene in the (S)TEM, an intriguing etching phenomenon was observed. The etching occurred in the microscope column in UHV conditions at room temperature. This behavior was distinct from

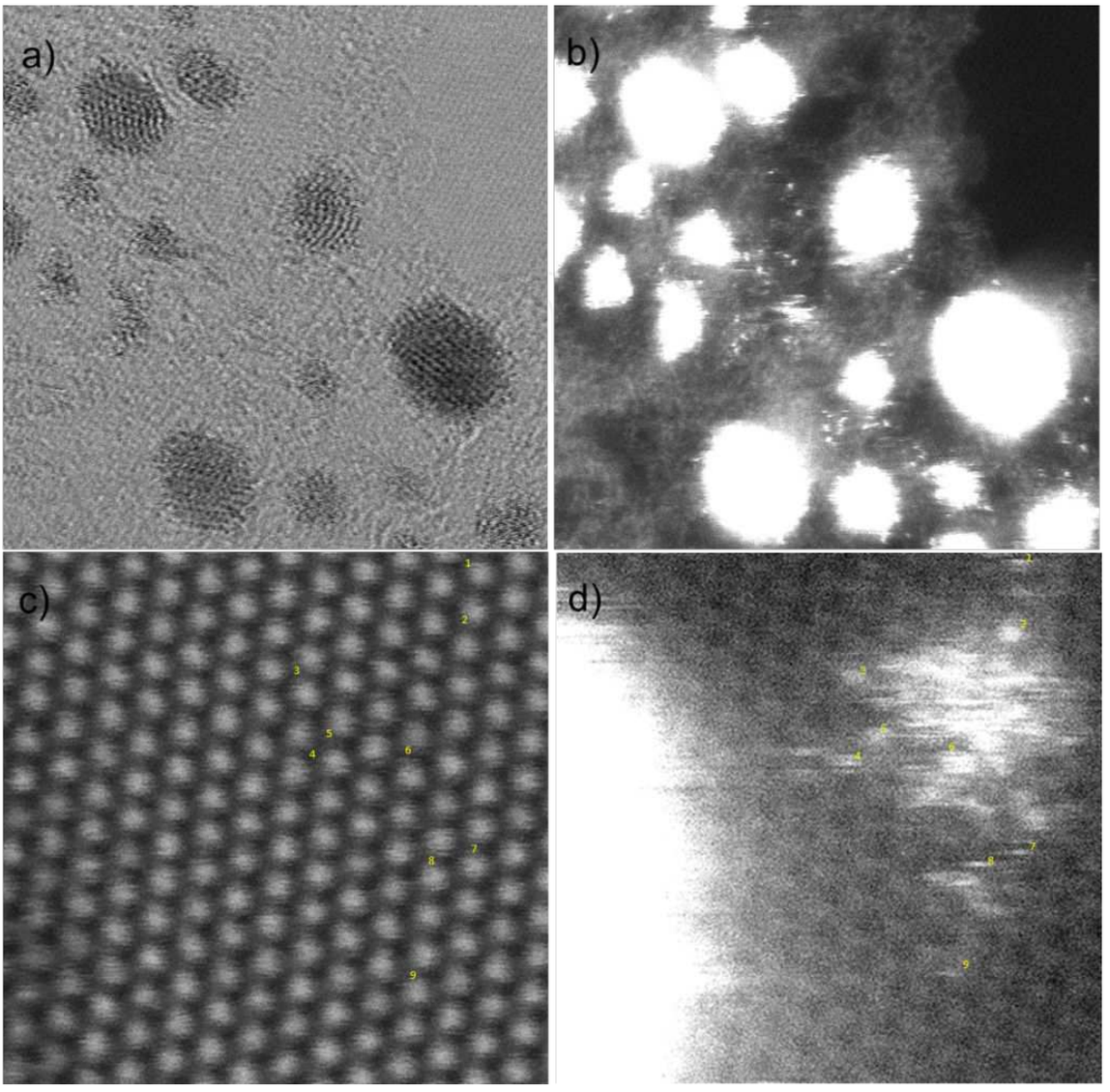


Figure 12. Unprocessed simultaneously taken a) BF and b) HAADF images of 2Å Au evaporated single layer graphene, simultaneously taken c) BF and d) HAADF images of 5Å Au evaporated few-layer graphene. All obtained at 60kV. Frame widths are 15 nm in a) and b) and 3nm in c) and d), respectively.

existing reports of graphene/graphite etching via metals at high temperature and under gas flow, a well-established method to cut graphitic layers [50, 51].

As seen in the images of figures 13 and 14a the metal clusters sit preferentially in the middle of the hydrocarbon contamination, however, after a few scans of the electron beam some of the clusters and/or individual atoms can be dragged by the beam to the edge of the contamination layer. Figure 14b shows an HAADF image of such a Ni cluster positioned in the middle of the contamination and figure 14c was taken after few scans that show the clusters were dragged to very edge of a contamination area. A magnified image of the red square in figure 14c is presented in figure 14d, which shows individual Ni atoms on a region of clean single layer graphene at the edge of the particle. While some carbon chains may still be present

http://dx.doi.org/10.5772/56640

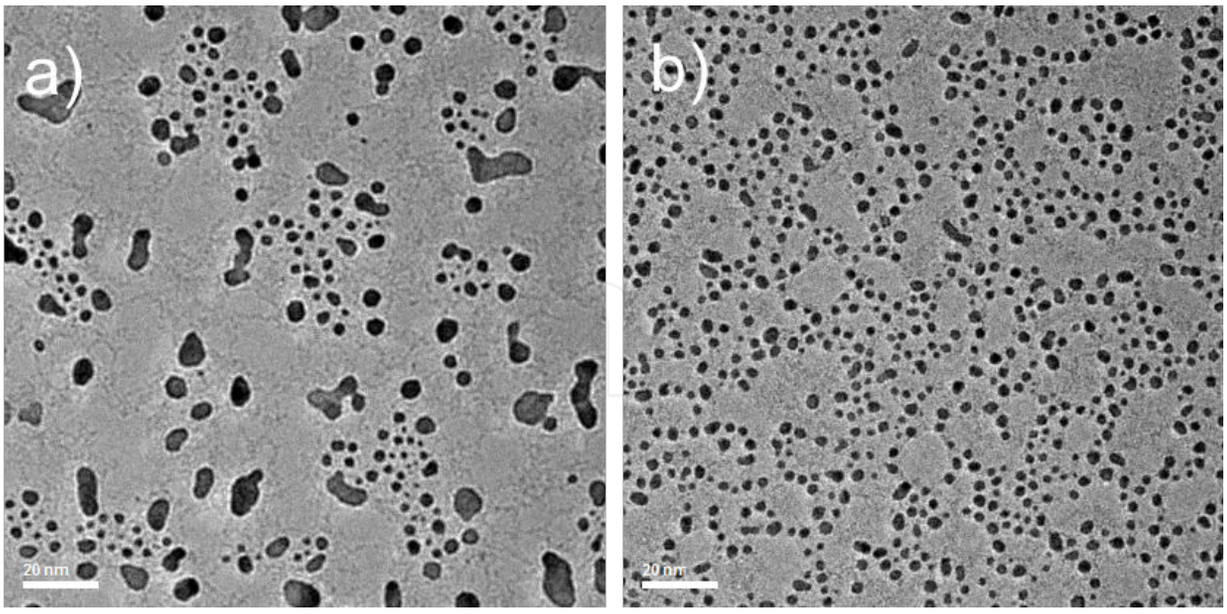


Figure 13. Unprocessed TEM images of 2Å gold evaporated onto a) pristine and b) hydrogenated graphene shown at the same magnification (the scale bar is 20 nm).

immediately under these Ni atoms, the here observed configuration offers a great proximity between pure graphene and metal atoms. After a few additional scans of the beam, a hole has formed (figure 14e), decorated by individual Ni atoms as evidenced by the clear Ni $M_{2,3}$ signature in the EEL spectrum (figure 14f), and acquired by placing the electron probe exactly on top of the bright atom marked in figure 14e. After the initial hole formation, individual Ni atoms are observed to jump onto the exposed edge with subsequent enlargement of the hole. The holes expand in proximity of the hydrocarbon contamination in which metal clusters reside. A strong indication that the drilling process is indeed metal-mediated arises from the observation that when no Ni atom is decorating the hole, the latter merely re-shapes dynamically but does not grow further in size. In other words, the drilling stops when the local reservoir of metal impurity atoms is exhausted, until more Ni atoms are drawn towards the energetically unstable edges of the hole *via* surface diffusion owing to the high mobility of single metal impurities on single layer graphene [52].

Further demonstration of the etching process which resulted in the hole evolution and expansion in the presence of metals (2Å Aluminum), is presented in figure 15. Figure 15a shows a clean, intact graphene patch (black) surrounded by hydrocarbons (gray) with Al clusters (white). Various stages of hole formation and enlargement are shown in subsequently taken images in figures 15b–d; figure 15e shows the hole after etching has more or less ceased. Once a hole is formed as result of interaction between Al atoms and graphene (figure 15b), the hole is decorated by newly arriving Al atoms, which are dragged by the electron beam, leading to further enlargement (figure 15c and d); no such atoms can be observed in figure 15e, indicating that the reservoir is exhausted. An overview at smaller magnification of an intermediate etching stage together with the aluminium distribution is shown in figure 15f. Figure 15 demonstrates clearly that the etching propagates from the border of the contamination into

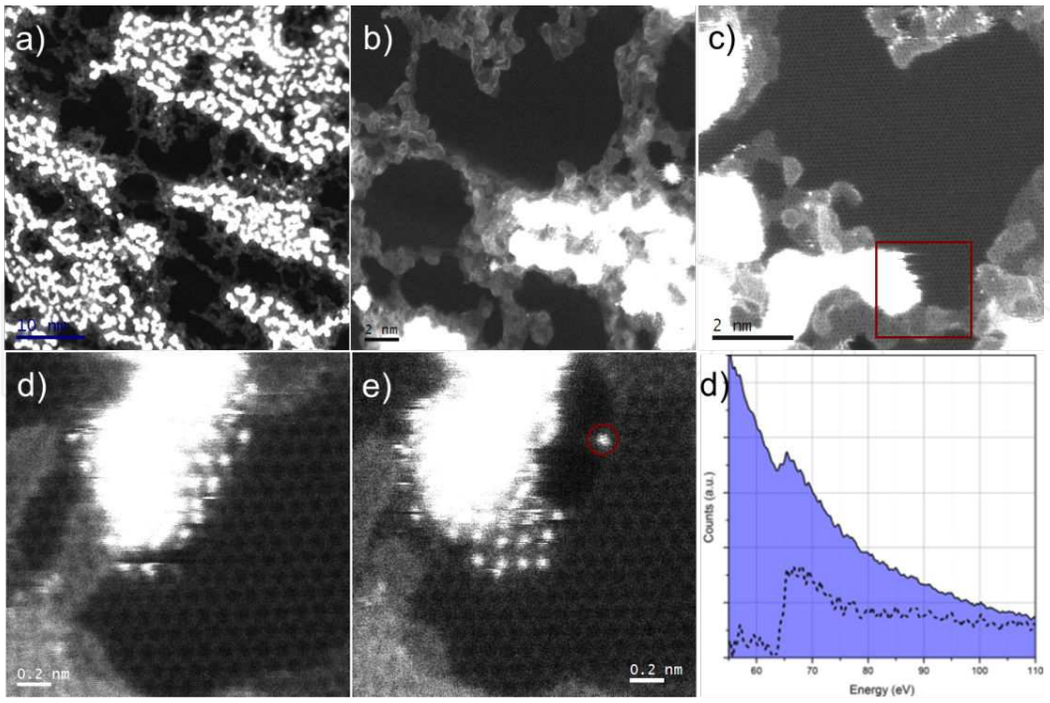


Figure 14. Unprocessed (a), (b) and (c) HAADF images of Ni clusters on graphene; (d) Ni-cluster sitting on the edge of the hydrocarbon contamination. Single Ni atoms have been dragged by the beam from the cluster and are in contact with the graphene single layer. (e) After a few more scans, a hole has formed, whose edges are decorated with single Ni atoms, identified by their Ni $M_{2,3}$ EELS signal, shown in f). EELS spectrum acquired by positioning the beam for 1s on the bright atom circled in (e)

clean graphene as long as metal atoms are supplied to the edge of the hole. In the absence of metal atoms at the hole, no progression of the etching is observed [53].

The migration of the metal atoms under the beam to the edge of the contamination layer and etching of graphene was observed for other metals on single layer graphene samples as well, e.g., for palladium (figure 16a) and titanium (figure 16b). In both cases, the nature of the atoms decorating the edges of the newly formed holes was confirmed by placing the electron probe directly on top of these atoms and recording an EELS spectrum, as shown on figure 16 below the corresponding HAADF images [52].

As mentioned earlier metals have been used as catalysts for patterning of graphene devices in hydrogen or oxygen flow at high temperatures [50, 54]. However, neither gas environment nor high temperatures were used in our study, which, to our knowledge, provides the first experimental evidence of electron beam- assisted drilling of graphene through direct interaction with metals. This destructive behavior was predicted specifically for Fe, Co, Ni and Al by calculations showing a drastic lowering of the formation energy for mono- and di-vacancies in single layer graphene when metal ad-atoms are present on the graphene surface [55]. In addition to that a constant trait of all those elements is their propensity to form oxides (except Au), which suggests that oxidation could be playing a major role in the effects we are observing. This hypothesis is further strengthened by the fact that by contrast no hole-forming was observed on Au-deposited samples, Au being of course not prone to oxidation except in very

http://dx.doi.org/10.5772/56640

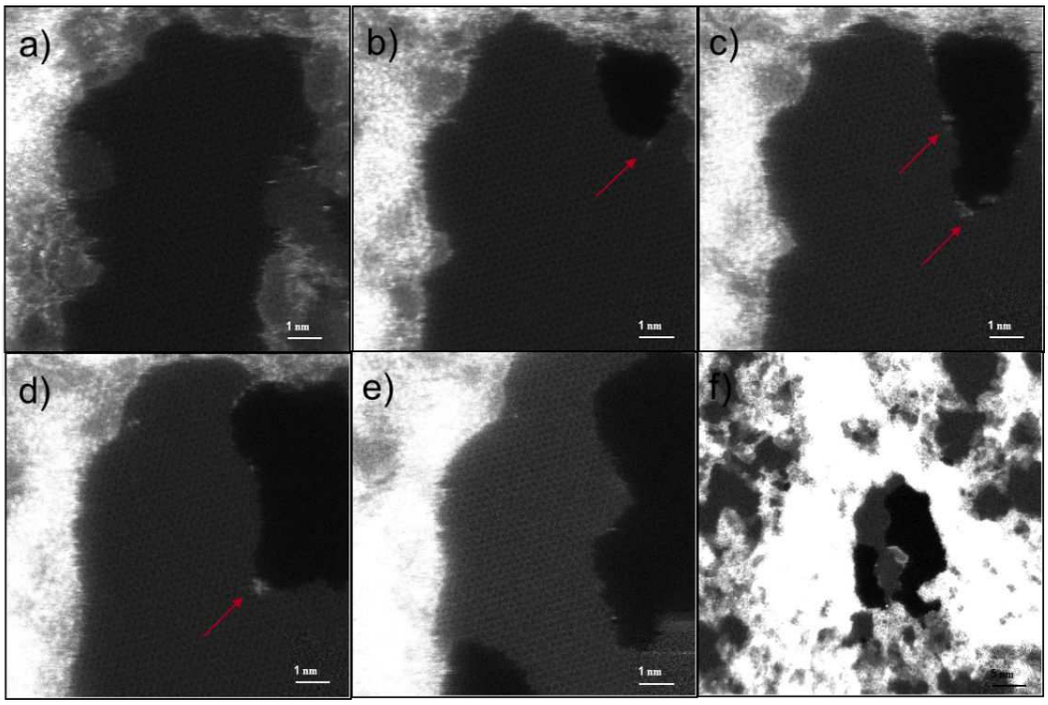


Figure 15. Unprocessed HAADF images of graphene etching in the presence of Al; (a) before etching, (b) after the start of the hole formation, (c) after hole enlargement in subsequent scans, (d) after continued etching as a result of a sustained supply of Al atoms to the hole's edge (some Al atoms are indicated by red arrows in (b–d), and (e) after the etching process has almost stopped because the Al atom supply has ceased; (f) lower magnification overview of the Al distribution and hole evolution. The scale bar is the same in (a–e), 1 nm.

specific circumstances. Nevertheless, even in the mono-vacancy formation model for the destruction of graphene proposed via DFT calculations Au is not expected to lead to a major loss in stability as its defect formation energy remains high so this observation cannot definitively point to a role of O in this etching process. The most likely sources of oxygen could be metal evaporation (relatively poor vacuum condition, ~10^{-7} torr), transport of the samples (exposing the sample to the air), hydrocarbon contamination (on the sample) and residual O_2 gases in the microscope column (with relatively high partial pressure of O). However, the latter can be ignored as the sample chamber (microscope column) was systematically at its base pressure of <$5x10^{-9}$torr.

7. Metal-h-BN interactions

Our metal-graphene interaction studies have inspired us to carry out micro structural studies of the metal-h-BN system to compare metal behaviors between these 2D systems. Similar to the graphene case Au, Ti and Ni metals have been investigated on the h-BN flakes.

Figure 17 shows simultaneously taken STEM- HAADF and BF images of 1Å gold evaporated on few-layer h-BN. Neither individual gold atoms nor clusters were observed on pristine parts of the h-BN sheets. However, ad-atoms and gold clusters can be seen in the hydrocarbon

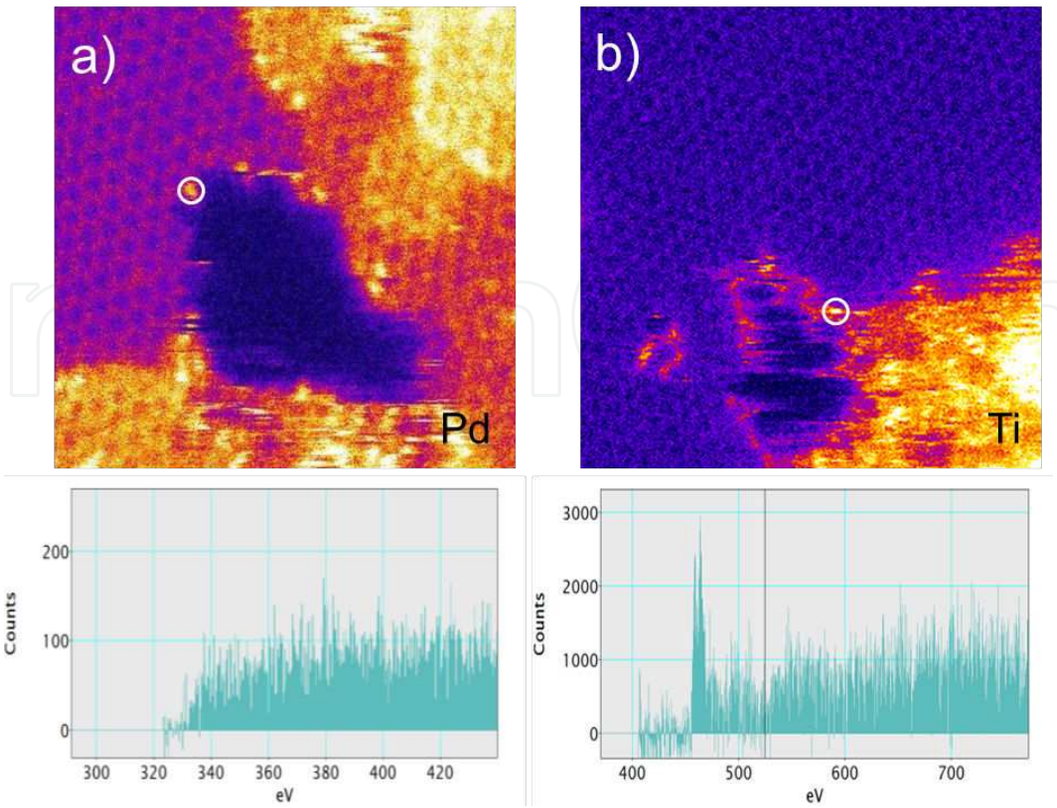


Figure 16. Unprocessed HAADF images (color inverted) of holes formed in single layer graphene through metal mediated etching with (a) Pd and (b) Ti. EEL spectra acquired by positioning the beam for 1s on the atoms encircled in the images are shown below the corresponding image.

contamination, which resembles the Au behavior on the graphene surfaces. This indicates the extreme mobility of gold on the clean h-BN surface. Single gold atoms have been observed in contaminated areas, as a result of dissociation from bigger gold cluster by the scanning beam in the STEM; these can be seen in figure 17a around the middle cluster, but no atoms can be seen on the clean h-BN surfaces. Another observation is the 'peeling' of BN layers under the continuous scanning electron beam. This has been shown earlier: the holes that occur are triangular in shape as indicated by the dashed white triangle in the HAADF image in figure 17a and in the corresponding BF image in figure 17b.

Another metal, which has been evaporated onto h-BN layers for comparison with graphene, is Ti as it has the highest coverage among the studied metals on the graphene surfaces for the same amount of metal. HAADF images of 1Å Ti evaporated double layer h-BN are shown in figure 18. A low magnification overview image in figure 18a shows the distribution of Ti on the h-BN surface. Ti is clustered and resides in the hydrocarbon chains similar to the graphene case, however, the distribution is less homogeneous compare to the Ti on graphene. A close-up image of figure 18a is shown in figure 18b; here the position of the Ti atoms and clusters can be clearly seen in the upper-right corner of the image. Although these clusters are dissociated and have moved towards edge of the hydrocarbon chains (bordering clean h-BN regions) during the scan, h-BN etching was not observed. This is in contrast to the Ti-graphene

http://dx.doi.org/10.5772/56640

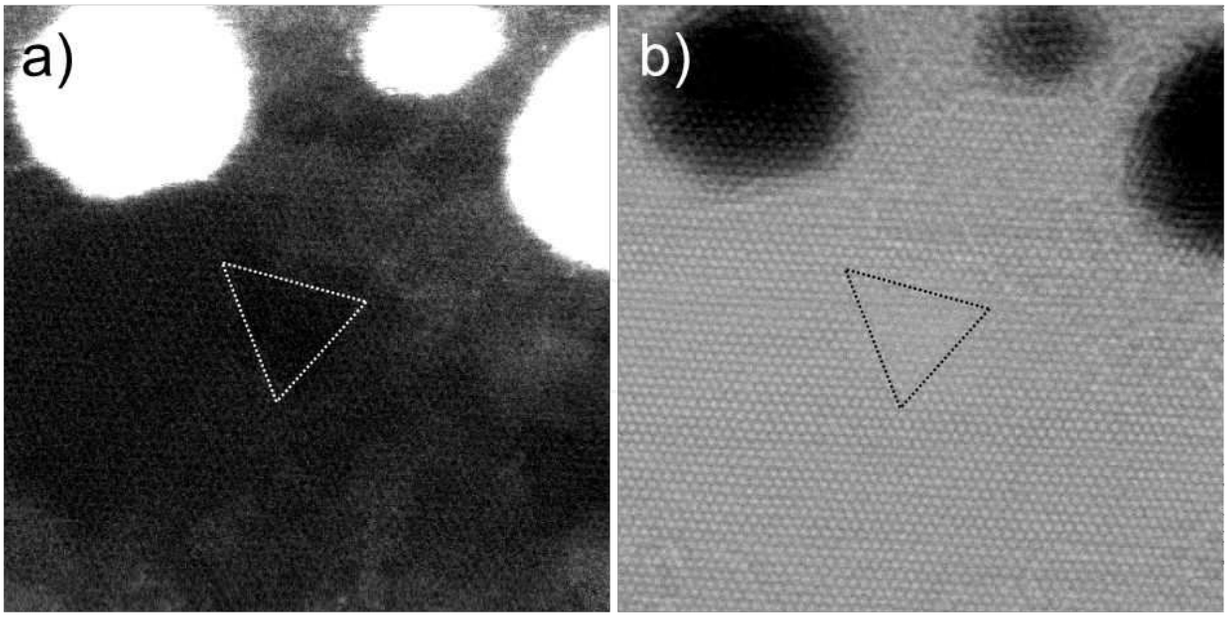


Figure 17. Unprocessed a) HAADF, b) BF image of 1Å Au doped h-BN, obtained at 100kV. Frame widths are 15nm.

interaction. Etching of h-BN as observed in both, figures 18b and c, is beam induced (knock-on damage), and is not metal mediated or related. Further evidenced for this is that it was not observed on the edge of the hydrocarbon chains, where the etching initiated in the case of metal-graphene interactions.

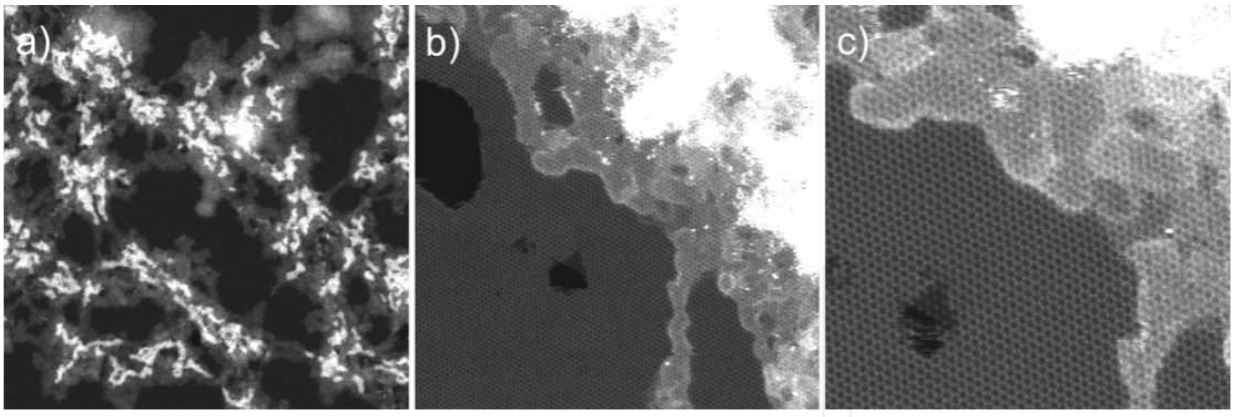


Figure 18. Unprocessed HAADF of 1Å Ti doped h-BN at different magnification, obtained at 60kV.

HAADF images of 1Å Ni doped h-BN and simultaneously taken corresponding BF images are shown in figure 19. Figures 19a, b and c are subsequently acquired HAADF images with increasing magnification at 60 kV acceleration voltage; magnified areas are indicated by blue squares in figures 19a and b. All HAADF images clearly show that there are no Ni atoms or cluster on clean h-BN surfaces. This is not obvious in the corresponding BF images, which reveal disturbances (Ni-islands) of the h-BN lattice; the impurities are in fact not sitting on the

h-BN lattice itself, but in/on the contamination layer between Ni atoms and the h-BN surface. Exact Ni-atom positions can only be revealed in the HAADF images, which is the reason why HAADF imaging is more powerful than phase contrast (BF) imaging in terms of revealing constellations and positions of impurities and ad-atoms. In particular, individual Ni atoms can be observed in the HAADF image in figure 19c to sit on a very fine contamination layer, through which the h-BN structure is still clearly visible. Without the guidance of the HAADF images it would not be possible to identify the sites of the ad-atoms on the honeycomb structure.

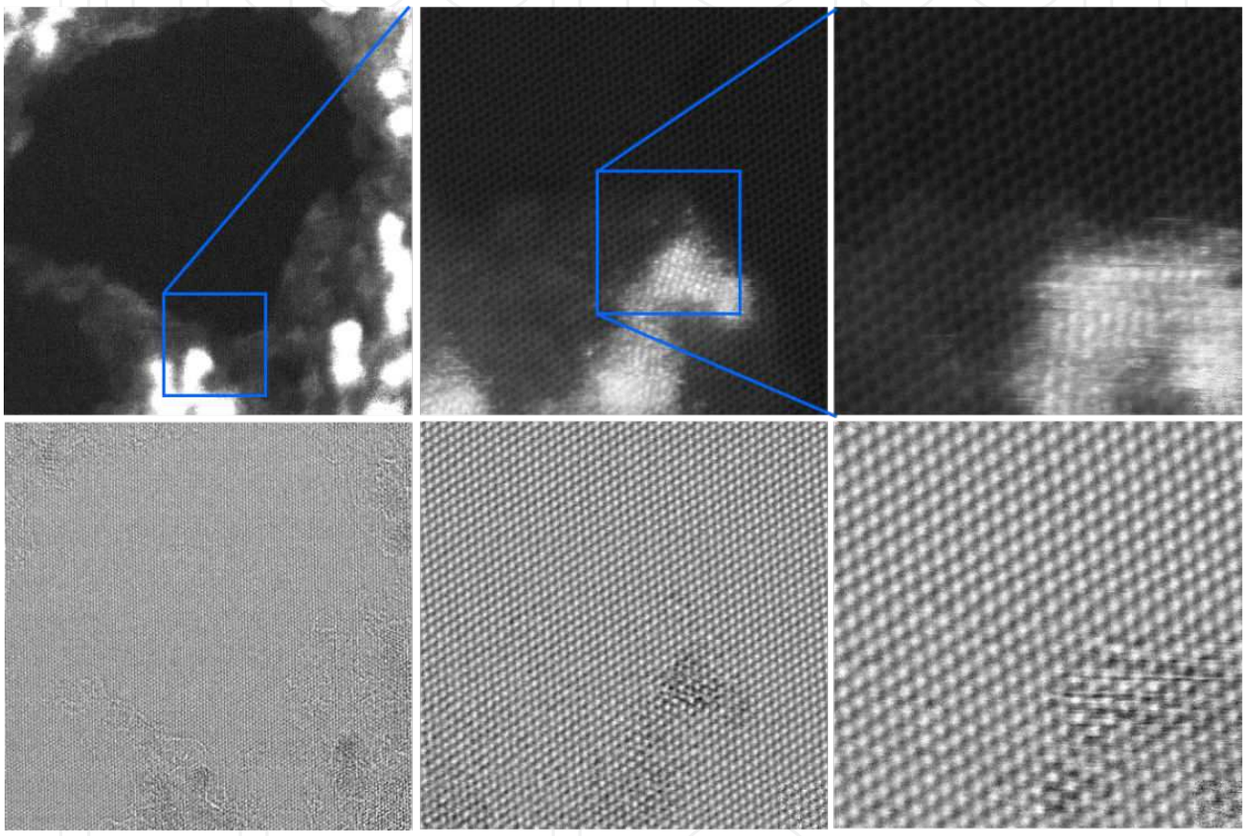


Figure 19. Unprocessed HAADF and BF images of 1Å Ni doped BN at different magnification, obtained at 60kV. a), b) and c) HAADF, d), e) and f) corresponding BF images. Frame widths are 25, 10, 5 nm in a) and b), c) and d), e) and f), respectively.

8. Conclusions

In conclusion, we used an aberration-corrected STEM, to investigate the structural properties of pristine graphene and h-BN layers on the atomic scale, and additionally the metal behaviors on these layers in terms of coverage, distribution and interaction.

Graphene and h-BN layer identification and atomic scale investigations were performed in TEM and STEM. We have shown that graphene and h-BN layers are not perfectly clean and

http://dx.doi.org/10.5772/56640

the presence of hydrocarbon contamination appears to be an issue with graphene structures in that it might has an effect on the charge transfer between graphene and metals. Single, two and few layer graphene were differentiated via diffraction patterns as was turbostratic graphene and the rotation angles between the layers. Hexagonal periodicity and individual carbon, boron and nitrogen atoms in graphene and h-BN layers were observed in TEM and STEM operated at an acceleration voltage below the knock-on threshold of carbon. Cleanliness, surface contamination and foreign ad-atoms on the graphene layers were identified in HAADF and EELS in the STEM.

After studies of pristine graphene in the (S)TEM, the behavior of the metals Au; Cr; Ti; Ni; Al; Pd on suspended graphene and Au; Ti; Ni on h-BN surfaces was investigated. As a general observation, all studied metals did not interact with the clean graphene and h-BN surface as none of them were observed on clean parts of them. The metals were mainly clustered and found to be on the hydrocarbon chains. The size and distribution of the clusters were found to vary on the graphene for different metals, for example Au clusters were the biggest and Ti the smallest in size for the same amount of metal deposition, which indicates that Ti has a better distribution than Au. Unequal distributions and irregular sizes of Au clusters were amended upon chemical modification of the graphene via hydrogenation. However, Au ad-atoms or clusters were still not observed on clean part of the graphene similar to the pristine case. The weak interaction between the metal and graphene and the preponderance of metals to reside on the hydrocarbons might have effects on the electrical transport properties of graphene (charge transfer between graphene and metals), because the hydrocarbon contamination on the graphene surface is unavoidable unless annealed at high temperatures and kept in UHV.

On the other hand, interesting results have been witnessed for all studied metals (except Au) in that they etch the graphene layer during STEM investigations. Although the metals nucleated on the hydrocarbons they were dragged by the scanning electron beam to clean parts of the graphene surface. As soon as the metal interacted with carbon atoms of the graphene a vacancy appeared followed by creation of further vacancies which coalesce to form a hole. This was observed although the microscope column was kept in UHV and operated at 60 kV, i.e., below the damaging threshold of carbon. Although it is known that the defect formation energies in graphene are substantially lowered in the mere presence of metal atoms, the actual etching mechanism at play here is not fully resolved. An oxidation mechanism may provide the most likely explanation, whereby oxygen released from nearby contamination may lead to a C-C bond dissociation mediated by the oxidation of the metal atoms. Furthermore, the observed metal-mediated etching of graphene could provide an explanation for the degradation of device performance over time. This etching could also be exploited in controlled tailoring and self-assembly processes for future graphene based devices as the etched holes can be healed spontaneously.

HAADF images reveal that both Au, Ti and Ni metals do not stick to the clean (contamination-free) surface of h-BN, however, they form ad-atoms and clusters on the contamination. That indicates the interaction between metals and BN is much weaker than the metal-metal interaction. On the other hand, we haven't observed any metal-mediated h-BN etching at all

in contrast to metal-graphene systems (even metals cannot be dragged towards clean bits under continuous scanning electron beam). That can be explained with the tendency of graphene to oxidation with yields of CO or CO_2 as the contaminations (even metal clusters) are rich from oxygen. It was also found that h-BN is a very good transparent support for the study of nanocrystals in the S/TEM.

Author details

Recep Zan[1,2*], Quentin M. Ramasse[3], Rashid Jalil[2] and Ursel Bangert[1]

*Address all correspondence to: recep.zan@manchester.ac.uk

1 School of Materials, The University of Manchester, Manchester, UK

2 School of Physics and Astronomy The University of Manchester, Manchester, UK

3 SuperSTEM Laboratory, STFC Daresbury Campus, Daresbury, UK

References

[1] Novoselov KS, Geim AK, Morozov SV, Jiang D, Zhang Y, Dubonos SV, et al. Electric Field Effect in Atomically Thin Carbon Films. Science. 2004 October 22, 2004;306(5696):666-9.

[2] Novoselov KS, Jiang D, Schedin F, Booth TJ, Khotkevich VV, Morozov SV, et al. Two-dimensional atomic crystals. Proceedings of the National Academy of Sciences of the United States of America. 2005;102(30):10451-3.

[3] Geim AK, Novoselov KS. The rise of graphene. Nat Mater. 2007;6(3):183-91.

[4] Xia F, Farmer DB, Lin Y-m, Avouris P. Graphene Field-Effect Transistors with High On/Off Current Ratio and Large Transport Band Gap at Room Temperature. Nano Letters. 2010;10(2):715-8.

[5] Dean CR, Young AF, Meric I, Lee C, Wang L, Sorgenfrei S, et al. Boron nitride substrates for high-quality graphene electronics. Nat Nano. 2010;5(10):722-6.

[6] Britnell L, Gorbachev RV, Jalil R, Belle BD, Schedin F, Mishchenko A, et al. Field-Effect Tunneling Transistor Based on Vertical Graphene Heterostructures. Science. 2012;335(6071):947-50.

[7] Jin C, Lin F, Suenaga K, Iijima S. Fabrication of a Freestanding Boron Nitride Single Layer and Its Defect Assignments. Physical Review Letters. 2009;102(19):195505.

[8] Novoselov KS, Falko VI, Colombo L, Gellert PR, Schwab MG, Kim K. A roadmap for graphene. Nature. 2012;490(7419):192-200.

[9] Bae S, Kim H, Lee Y, Xu X, Park J-S, Zheng Y, et al. Roll-to-roll production of 30-inch graphene films for transparent electrodes. Nat Nano. 2010;5(8):574-8.

[10] Stoller MD, Park S, Zhu Y, An J, Ruoff RS. Graphene-Based Ultracapacitors. Nano Letters. 2008;8(10):3498-502.

[11] Yoo E, Kim J, Hosono E, Zhou H-s, Kudo T, Honma I. Large Reversible Li Storage of Graphene Nanosheet Families for Use in Rechargeable Lithium Ion Batteries. Nano Letters. 2008;8(8):2277-82.

[12] Grigorenko AN, Polini M, Novoselov KS. Graphene plasmonics. Nat Photon. 2012;6(11):749-58.

[13] Stankovich S, Dikin DA, Dommett GHB, Kohlhaas KM, Zimney EJ, Stach EA, et al. Graphene-based composite materials. Nature. 2006;442(7100):282-6.

[14] Schedin F, Geim AK, Morozov SV, Hill EW, Blake P, Katsnelson MI, et al. Detection of individual gas molecules adsorbed on graphene. Nat Mater. 2007;6(9):652-5.

[15] Pantelic RS, Meyer JC, Kaiser U, Stahlberg H. The application of graphene as a sample support in transmission electron microscopy. Solid State Communications. 2012;152(15):1375-82.

[16] Pi K, McCreary KM, Bao W, Han W, Chiang YF, Li Y, et al. Electronic doping and scattering by transition metals on graphene. Physical Review B. 2009;80(7):075406.

[17] Bolotin KI, Sikes KJ, Jiang Z, Klima M, Fudenberg G, Hone J, et al. Ultrahigh electron mobility in suspended graphene. Solid State Communications. 2008;146:351-5.

[18] Zan R, Muryn C, Bangert U, Mattocks P, Wincott P, Vaughan D, et al. Scanning tunnelling microscopy of suspended graphene. Nanoscale. 2012;4(10):3065-8.

[19] Morozov SV, Novoselov KS, Katsnelson MI, Schedin F, Elias DC, Jaszczak JA, et al. Giant Intrinsic Carrier Mobilities in Graphene and Its Bilayer. Physical Review Letters. 2008;100(1):016602.

[20] Meyer JC, Geim AK, Katsnelson MI, Novoselov KS, Booth TJ, Roth S. The structure of suspended graphene sheets. Nature. 2007;446(7131):60-3.

[21] Gass MH, Bangert U, Bleloch AL, Wang P, Nair RR, Geim AK. Free-standing graphene at atomic resolution. Nat Nano. 2008;3(11):676-81.

[22] Krivanek OL, Dellby N, Murfitt MF, Chisholm MF, Pennycook TJ, Suenaga K, et al. Gentle STEM: ADF imaging and EELS at low primary energies. Ultramicroscopy. 2010;110(8):935-45.

[23] Gorbachev RV, Riaz I, Nair RR, Jalil R, Britnell L, Belle BD, et al. Hunting for Monolayer Boron Nitride: Optical and Raman Signatures. Small. 2010;7(4):465-8.

[24] Blake P, Hill EW, Neto AHC, Novoselov KS, Jiang D, Yang R, et al. Making graphene visible. Applied Physics Letters. 2007;91(6):063124-3.

[25] Li X, Cai W, An J, Kim S, Nah J, Yang D, et al. Large-Area Synthesis of High-Quality and Uniform Graphene Films on Copper Foils. Science. 2009 June 5, 2009;324(5932): 1312-4.

[26] Ago H, Ogawa Y, Tsuji M, Mizuno S, Hibino H. Catalytic Growth of Graphene: Toward Large-Area Single-Crystalline Graphene. The Journal of Physical Chemistry Letters. 2012;3(16):2228-36.

[27] Liang X, Sperling BA, Calizo I, Cheng G, Hacker CA, Zhang Q, et al. Toward Clean and Crackless Transfer of Graphene. ACS Nano. 2011 2012/11/21;5(11):9144-53.

[28] Suk JW, Kitt A, Magnuson CW, Hao Y, Ahmed S, An J, et al. Transfer of CVD-Grown Monolayer Graphene onto Arbitrary Substrates. ACS Nano. 2011 2012/11/21;5(9): 6916-24.

[29] Crewe AV. The physics of the high-resolution scanning microscope. Reports on Progress in Physics. 1980;43(5):621.

[30] Hartel P, Rose H, Dinges C. Conditions and reasons for incoherent imaging in STEM. Ultramicroscopy. 1996;63(2):93-114.

[31] Krivanek OL, Zhou W, Chisholm MF, Idrobo JC, Lovejoy TC, Ramasse QM, et al. Gentle STEM of Single Atoms: Low keV Imaging and Analysis at Ultimate Detection Limits. Low Voltage Electron Microscopy: John Wiley & Sons, Ltd; 2012. p. 119-61.

[32] Krivanek OL, Chisholm MF, Nicolosi V, Pennycook TJ, Corbin GJ, Dellby N, et al. Atom-by-atom structural and chemical analysis by annular dark-field electron microscopy. Nature. 2010;464(7288):571-4.

[33] Meyer JC, Geim AK, Katsnelson MI, Novoselov KS, Obergfell D, Roth S, et al. On the roughness of single- and bi-layer graphene membranes. Solid State Communications. 2007;143(1-2):101-9.

[34] Bangert U, Gass MH, Bleloch AL, Nair RR, Eccles J. Nanotopography of graphene. Physica Status Solidi (a). 2009;206(9):2115-9.

[35] Bangert U, Gass MH, Bleloch AL, Nair RR, Geim AK. Manifestation of ripples in free-standing graphene in lattice images obtained in an aberration-corrected scanning transmission electron microscope. Physica Status Solidi (a). 2009;206(6):1117-22.

[36] Girit CO, Meyer JC, Erni R, Rossell MD, Kisielowski C, Yang L, et al. Graphene at the Edge: Stability and Dynamics. Science. 2009 March 27, 2009;323(5922):1705-8.

[37] Banhart F, Kotakoski J, Krasheninnikov AV. Structural Defects in Graphene. ACS Nano. 2011;5(1):26-41.

[38] Zan R, Bangert U, Ramasse Q, Novoselov KS. Imaging of Bernal stacked and misoriented graphene and boron nitride: experiment and simulation. Journal of Microscopy. 2011;244(2):152-8.

[39] Warner JH, Rummeli MH, Gemming T, Buchner B, Briggs GAD. Direct Imaging of Rotational Stacking Faults in Few Layer Graphene. Nano Letters. 2008;9(1):102-6.

[40] Meyer JC, Kisielowski C, Erni R, Rossell MD, Crommie MF, Zettl A. Direct Imaging of Lattice Atoms and Topological Defects in Graphene Membranes. Nano Letters. 2008;8(11):3582-6.

[41] Chuvilin A, Meyer C. J, Algara-Siller G, Kaiser U. From graphene constrictions to single carbon chains. New Journal of Physics. 2009;11(8):083019.

[42] Haigh SJ, Gholinia A, Jalil R, Romani S, Britnell L, Elias DC, et al. Cross-sectional imaging of individual layers and buried interfaces of graphene-based heterostructures and superlattices. Nat Mater. 2012;11(9):764-7.

[43] Kirkland EJ. Advanced Computing in Electron Microscopy. 1. ed.: Plenum Press; 1998.

[44] Hass J, Varchon F, Millan-Otoya JE, Sprinkle M, Sharma N, de Heer WA, et al. Why Multilayer Graphene on 4H-SiC(0001) Behaves Like a Single Sheet of Graphene. Physical Review Letters. 2008;100(12):125504.

[45] Pong W-T, Durkan C. A review and outlook for an anomaly of scanning tunnelling microscopy (STM): superlattices on graphite. Journal of Physics D: Applied Physics. 2005;38(21):R329-55.

[46] Meyer JC, Chuvilin A, Algara-Siller G, Biskupek J, Kaiser U. Selective Sputtering and Atomic Resolution Imaging of Atomically Thin Boron Nitride Membranes. Nano Letters. 2009;9(7):2683-9.

[47] Zan R, Bangert U, Ramasse Q, Novoselov KS. Metal-Graphene Interaction Studied via Atomic Resolution Scanning Transmission Electron Microscopy. Nano Letters. 2011;11(3):1087-92.

[48] Zan R, Bangert U, Ramasse Q, Novoselov KS. Evolution of Gold Nanostructures on Graphene. Small. 2011;7(20):2868-72.

[49] Erni R, Rossell MD, Nguyen M-T, Blankenburg S, Passerone D, Hartel P, et al. Stability and dynamics of small molecules trapped on graphene. Physical Review B. 2010;82(16):165443.

[50] Campos LC, Manfrinato VR, Sanchez-Yamagishi JD, Kong J, Jarillo-Herrero P. Anisotropic Etching and Nanoribbon Formation in Single-Layer Graphene. Nano Letters. 2009;9(7):2600-4.

[51] Booth TJ, Pizzocchero F, Andersen H, Hansen TW, Wagner JB, Jinschek JR, et al. Discrete Dynamics of Nanoparticle Channelling in Suspended Graphene. Nano Letters. 2011;11(7):2689-92.

[52] Ramasse QM, Zan R, Bangert U, Boukhvalov DW, Son Y-W, Novoselov KS. Direct Experimental Evidence of Metal-Mediated Etching of Suspended Graphene. ACS Nano. 2012;6(5):4063-71.

[53] Zan R, Bangert U, Ramasse Q, Novoselov KS. Interaction of Metals with Suspended Graphene Observed by Transmission Electron Microscopy. The Journal of Physical Chemistry Letters. 2012 2012/03/22;3:953-8.

[54] Severin N, Kirstein S, Sokolov IM, Rabe JP. Rapid Trench Channeling of Graphenes with Catalytic Silver Nanoparticles. Nano Letters. 2008;9(1):457-61.

[55] Boukhvalov, D. W.; Katsnelson, M. I. Destruction of Graphene by Metal Adatoms. Appl. Phys. Lett. 2009, 95, 023109.

IntechOpen